Search for a Variation of the Fine Structure around the Supermassive Black Hole in Our Galactic Center

A. Hees,[1,*] T. Do,[2] B. M. Roberts,[1,3] A. M. Ghez,[2] S. Nishiyama,[4] R. O. Bentley,[2] A. K. Gautam,[2] S. Jia,[5] T. Kara,[4] J. R. Lu,[5] H. Saida,[6] S. Sakai,[2] M. Takahashi,[7] and Y. Takamori[8]

[1] *SYRTE, Observatoire de Paris, Université PSL, CNRS, Sorbonne Université, LNE, 61 avenue de l'Observatoire 75014 Paris, France*
[2] *Department of Physics and Astronomy, University of California, Los Angeles, California 90095, USA*
[3] *School of Mathematics and Physics, The University of Queensland, Brisbane, QLD 4072, Australia*
[4] *Miyagi University of Education, 149 Aramaki-aza-aoba, Aoba-ku, Sendai, Miyagi 980-0845, Japan*
[5] *Astronomy Department, University of California, Berkeley, CA 94720, USA*
[6] *Daido University, 10-3 Takiharu-cho, Minami-ku, Nagoya, Aichi 457-8530, Japan*
[7] *Aichi University of Education, 1 Hirosawa, Igaya-cho, Kariya, Aichi 448-8542, Japan*
[8] *National Institute of Technology, Wakayama College, 77 Noshima, Nada-cho, Gobo, Wakayama 644-0023, Japan*

Searching for space-time variations of the constants of Nature is a promising way to search for new physics beyond General Relativity and the standard model motivated by unification theories and models of dark matter and dark energy. We propose a new way to search for a variation of the fine-structure constant using measurements of late-type evolved giant stars from the S-star cluster orbiting the supermassive black hole in our Galactic Center. A measurement of the difference between distinct absorption lines (with different sensitivity to the fine structure constant) from a star leads to a direct estimate of a variation of the fine structure constant between the star's location and Earth. Using spectroscopic measurements of 5 stars, we obtain a constraint on the relative variation of the fine structure constant below 10^{-5}. This is the first time a varying constant of Nature is searched for around a black hole and in a high gravitational potential. This analysis shows new ways the monitoring of stars in the Galactic Center can be used to probe fundamental physics.

The current understanding of our Universe is based on the theory of General Relativity (GR) and on the Standard Model (SM) of particle physics. While both theories have been extremely successful, they are expected to break down at a certain point. In particular, a breaking of the Einstein equivalence principle is expected in various unification scenarios [1, 2], in higher dimensional theories [3], and by some models of dark matter [4, 5] and dark energy [6, 7]. On a more philosophical note, the "principle of absence of absolute structure" led to many developments of extensions of physics where the constants of physics become dynamical entities, explicitly breaking the equivalence principle (see the discussion in section 2 of [8]).

One way to test the equivalence principle is to search for space-time variations of the constants of Nature such as the fine structure constant α, the mass of fermions and the quantum chromodynamics energy scale (see [9] for a review of the tests of GR and [10] for a review of the search for varying constants). Various experiments using atomic clocks have provided stringent constraints on linear drifts of the constants of Nature at the level of 10^{-16} yr^{-1} [11–18], on a dependency of the constants of Nature to the Sun gravitational potential at the level of 10^{-7} [14–16, 19, 20] or on harmonic variations of the constants of Nature [21]. A time variation of α has also been searched for using measurements of quasar absorption spectra [22] providing constraint on $\Delta\alpha/\alpha$ at the level of 10^{-6} for cosmological redshift up to $z \sim 3$. A variation of α has also been constrained at the level of 10^{-3} for $z \sim 10^3$ using cosmic microwave background measurements [23] and at a similar level for $z \sim 10^{10}$ by a big bang nucleosynthesis analysis [24]. Finally, a dependency of α on the gravitational potential has also been searched for using absorption lines from a white dwarf [25]. Although many searches for a variation of α have been performed, the question of its constancy around a black hole and around a supermassive body remains totally open.

The motion of the short-period stars (S-stars) orbiting around the $4 \times 10^6\, M_\odot$ supermassive black hole (SMBH) at the center of our Galaxy has been monitored for 25 years by two experiments: one carried out at the Keck Observatory [26–28] and the other with the New Technology Telescope (NTT) and with the Very Large Telescope (VLT) [29–31]. Recently, these measurements have opened a new window to probe fundamental physics around a SMBH. Measurements of the short-period star S0-2/S2 have been used to search for a fifth interaction [27, 32], to measure the relativistic redshift during its 2018 closest approach [28, 30] and to perform a null-redshift test [31].

In this Letter, we present a novel search for variations of the fine structure constant around a SMBH using spectroscopic measurements from late-type evolved giant stars orbiting Sagittarius A* (Sgr A*). This is the first search for a varying α around a compact object (the compactness of a celestial body can be characterized by $\Xi = GM/c^2R$ with R the body's radius) and very massive object, exploring a new region in the pa-

* aurelien.hees@obpsm.fr

rameter space (Fig. 1). Probing the gravitational interaction in such a region is important to test for theories which exhibit screening mechanism in the solar system (see e.g. [6, 33, 34]) or for theories that exhibit a scalarization mechanism around a black hole [35].

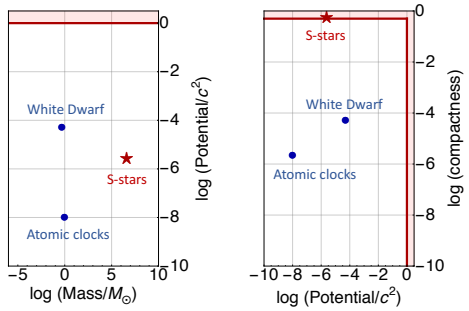

FIG. 1. Left: the gravitational potential probed by several searches for varying α against the mass of the central body that generates gravity in these tests. Right: the compactness $\Xi = GM/c^2R$ of the central body probed by several searches for varying α against the gravitational potential. Searches for varying α with S-stars explore a new region in this parameter space.

Using spectroscopy, we can very precisely measure the wavelengths of atomic lines, which can be used to measure potential variations in the the fine structure constant. The spectroscopic observable is given by

$$\frac{\Delta\lambda_j}{\lambda_j} = \frac{\lambda_j(z,\alpha) - \lambda_j(z=0,\alpha_0)}{\lambda_j(z=0,\alpha_0)} = z - k_{\alpha,j}(1+z)\frac{\Delta\alpha}{\alpha}\,, \tag{1}$$

where $\lambda_j(z,\alpha)$ is the measured central wavelength of an absorption line j at the GC for a value of α potentially different from the one on Earth α_0 while $\lambda_j(0,\alpha_0)$ is the wavelength for the same line measured in the lab. In this expression, z is the traditional Doppler shift (which includes the Newtonian velocity along the line of sight and the relativistic corrections on the redshift) and the last term encodes the impact due to a variation of α on the measurements. This term depends directly on $k_{\alpha,j}$, the sensitivity of the transition j to α and defined by

$$d\ln\nu_j = k_{\alpha,j}\, d\ln\alpha\,, \tag{2}$$

where $\nu_j = c/\lambda_j$ is the frequency of the absorption line j.

Late-type evolved stars are particularly useful for such an analysis because their cool atmospheres result in spectra that contain many strong atomic absorption lines which helps to maximize the number of different lines available for this analysis. Also importantly, their spectra contain lines that are related to atomic transitions with different sensitivity to α (the difference between the k_α coefficients are of the order of 1). In comparison, the more well studied young early-type S-stars such as S0-2 have atmospheres that are very hot, so their Near-Infrared (NIR) spectra contain only a few H and He absorption. Unfortunately, H and He lines have nearly the same sensitivity to α (the difference between the k_α coefficients are of the order of 10^{-5}) making these lines insensitive to the effect of variations in α.

In this work, we focus on 5 late-type giants in orbit around the supermassive black hole: S0-6, S0-12, S0-13, S1-5 and S1-23, see Fig. 2 and [36]. These are among the closest late-type stars to the black hole (0.4 to 1.5 arcseconds in projection) with NIR spectroscopic measurements. Observations of these stars include imaging data from Keck Observatory and spectroscopic data from Gemini North, Keck Observatory and Subaru telescope. The imaging data include both speckle imaging from the Near-Infrared Camera (NIRC) instrument (1995-2005) and adaptive optics data from the Near-Infrared Camera 2 (NIRC2) instrument (2005-2018). Details of the data reduction are given in [28]. NIR spectra were obtained with the Near-Infrared Integral Field Spectrometer (NIFS) instrument on Gemini North for the stars S0-6, S0-12, S0-13, and S1-5 using the K-band filter (0.95 to 2.40 μm) at a spectral resolution $R = \lambda/\Delta\lambda = 5000$. We use spectra of these stars taken on May 13 and May 22, 2018. Additional spectroscopy of the star S0-6 was obtained using the Infrared Camera and Spectrograph (IRCS) instrument from Subaru. We use the the order 26 spectrum (2.16 to 2.22 μm) at a resolution of R = 20,000 (down-sampled to R = 15000) for this work. Details of the data reduction for IRCS is given in [37] and [38]. Spectroscopy of the star S1-23 was obtained using the NIRSPEC instrument with laser-guide-star adaptive optics at Keck Observatory at a spectral resolution R =20,000. NIRSPEC was used in echelle mode with the K-filter. We use Orders 34 (2.24 to 2.27 μm) and 35 (2.18 to 2.21 μm) for this work. Details of the data reduction for the NIFS data and NIRSPEC data are given in [28] and [39], respectively. All the NIFS, IRCS and NIRSPEC spectra have signal-to-noise ratios (SNR) greater than 20 in order to measure individual lines.

We identified a number of strong and sufficiently isolated absorption lines for this experiment (Fig. 3). In total, we measure 3 atomic lines from stars with NIFS spectra, 6 atomic lines with IRCS spectra, and 10 atomic lines from the NIRSPEC spectra (Tab. I). The higher spectral resolution from NIRSPEC compared to NIFS allows us to use more lines. We use a Gaussian fit to determine the central wavelength of each atomic transition and a Monte Carlo simulation to estimate the uncertainty. The fitted lines and uncertainties are reported in Sec. II from the Supplemental Material [40].

To determine the sensitivity coefficients k_α for each absorption line used in this study, we perform ab initio calculation of the spectrum for each element by solving the Dirac Hamiltonian in flat spacetime (curvature corrections are subdominant) and then compute k_α by a finite difference. The spectra are computed using a combination of the configuration interaction (CI) method with many-body perturbation theory (MBPT) [41–44] using

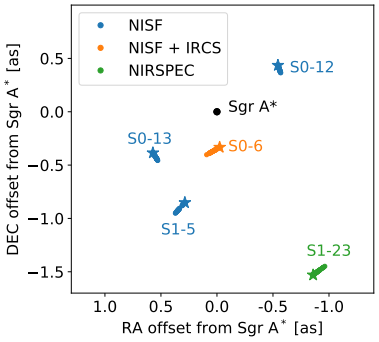

FIG. 2. Representation of the motion of the five stars considered in our analysis between 1995 and 2018. The large stars represent the positions of the stars in 2018. All these stars have a magnitude brighter than $M = 15$. S0-6, S0-12, S0-13, S1-5 have been measured spectroscopically with the NIFS instrument with Gemini in 2018, S0-6 was also measured with the IRCS instrument from Subaru in 2018 and S1-23 with the NIRSPEC instrument at Keck in 2016.

the AMBiT software [45]. The full details of the calculations are presented in Appendix A; here we just outline briefly the main aspects of the method. The effective wavefunctions for a M-valence atom are expanded as a series of M-body Slater-determinants, where the expansion coefficients are found variationally by minimizing the energy (CI method). To greatly improve the accuracy, the effects of core-valence electron correlations are also included into the valence wavefunctions. This is done by modifying the effective Hamiltonian for the valence states using MBPT before the CI procedure is performed. Finally, to calculate the k_α coefficients, we explicitly make small variations into value of the fine structure constant ($\alpha \to \alpha \pm \delta\alpha$) in the code before the equations are solved.

Bayesian inference is used to estimate $\Delta\alpha/\alpha$ from the measurements and Eq. (1). The measurement errors for each line are assumed to be independent and to be normally distributed such that the full likelihood is the product of the individual likelihoods

$$\mathcal{L}_j \propto \exp\left[-\frac{1}{2\sigma_j^2}\left(\frac{\Delta\lambda_j}{\lambda_j} - z + k_{\alpha,j}(1+z)\frac{\Delta\alpha}{\alpha}\right)^2\right], \quad (3)$$

where the subscript j refers to a particular line. Uniform priors for $\Delta\alpha/\alpha$ and for z are used and Gaussian priors are used for the sensitivity coefficients $k_{\alpha,j}$ with a mean value and an uncertainty quoted in Tab. I. We use the MULTINEST sampler [47] to sample the posterior probability distribution function. All the epochs are fitted simultaneously but offsets between the different instruments or filters are taken into account (this results in different fitted velocities for each instrument or filter).

No significant deviation of the fine structure constant is detected for any of the stars considered in this analysis. The posterior probability distributions for each star

TABLE I. Atomic properties of the absorption lines used in this analysis. The wavelengths λ are experimental values reported in [46]. The sensitivity to the fine structure constant k_α is computed from ab initio calculation using the AMBIT software [45], see the discussion in Appendix A. The last column indicates which instrument has been used to measured each line with: (a) NIFS spectrograph, (b) IRCS spectrograph, (c) NIRSPEC order34, (d) NIRSPEC order35.

	Lower		Upper		λ [Å]	k_α	Inst.
$_{14}$Si	$3s^23p4p$	$^1D_2$	$3s^23p5s$	$^1P_1^o$	21360.027	0.013(9)	a
$_{11}$Na	$4s$	$^2S_{1/2}$	$4p$	$^2P_{1/2}^o$	22089.728	0.004(2)	a,b
$_{22}$Ti	$3d^34s$	$^5P_2$	$3d^24s4p$	$^5D_2^o$	22238.911	-0.34(10)	a
$_{22}$Ti	$3d^34s$	$^5P_2$	$3d^24s4p$	$^5D_1^o$	22450.025	-0.37(10)	c
$_{39}$Y	$4d^25s$	$^4F_{7/2}$	$4d5s5p$	$^4F_{7/2}^o$	22549.938	-0.88(6)	c
$_{20}$Ca	$4s4d$	$^3D_1$	$4s4f$	$^3F_2^o$	22614.115	-0.03(1)	c
$_{21}$Sc	$3d^24s$	$^4F_{3/2}$	$3d4s4p$	$^2D_{3/2}^o$	21848.743	-0.23(3)	b,d
$_{39}$Fe	$3d^64s^2$	$^3D_3$	$3d^64s4p$	$^3P_2^o$	21857.345	0.56(28)	d
$_{22}$Ti	$3d^34s$	$^5P_2$	$3d^24s4p$	$^5D_3^o$	21903.353	-0.30(10)	b,d
$_{22}$Ti	$3d^34s$	$^5P_1$	$3d^24s4p$	$^5D_2^o$	22010.501	-0.31(9)	b,d
$_{21}$Sc	$3d^24s$	$^4F_{5/2}$	$3d4s4p$	$^2D_{3/2}^o$	22030.179	-0.25(4)	b,d
$_{21}$Sc	$3d^24s$	$^4F_{9/2}$	$3d4s4p$	$^4D_{7/2}^o$	22058.003	-0.29(4)	d
$_{11}$Na	$4s$	$^2S_{1/2}$	$4p$	$^2P_{3/2}^o$	22062.485	0.007(2)	b,d

can be found in Sec. IV from the supplemental material [40] and the 68% confidence intervals are reported in Tab. II. The constraints derived from the NIRSPEC measurements are one order of magnitude better than from the NIFS instrument due to the better spectral resolution and more atomic lines observed with NIRSPEC.

TABLE II. 68% confidence interval for $\Delta\alpha/\alpha$ and for z estimated from different stars. An estimation of the gravitational potential U at the location of the star is also provided (see Sec. III from the supplemental material [40]). For S0-12, S0-13 and S1-5, two NIFS measurement epochs are combined with 3 absorption lines per epoch. S0-6 has been observed with NIFS and IRCS (each instrument has a different wavelength solution which reflects in an offset in their estimated z value) providing 9 lines. S1-23 has been observed with two different filters (each filter has a different wavelength solution which reflects in an offset in their estimated z value) providing 10 absorption lines.

Star	$\frac{\Delta\alpha}{\alpha}$	$z.c$ [km/s]	U/c^2
S0-6	$(1.0 \pm 1.2) \times 10^{-4}$	71.0 ±10.4	2.4×10^{-6}
		−3.6 ±5.3	
S0-12	$(-0.3 \pm 1.4) \times 10^{-4}$	−57.3 ±4.6	1.6×10^{-6}
S0-13	$(0.03 \pm 3.5) \times 10^{-4}$	−61.6 ±18.1	9.4×10^{-7}
S1-5	$(-0.7 \pm 2.4) \times 10^{-4}$	−3.7 ±19.4	6.5×10^{-7}
S1-23	$(0.9 \pm 5.8) \times 10^{-6}$	−311.4 ±1.1	4.6×10^{-7}
		288.1 ±0.7	

A fit combining all the stars using a global likelihood (see Sec. IV from the supplemental material [40] for more details) provides a constraint of

$$\frac{\Delta\alpha}{\alpha} = (1.0 \pm 5.8) \times 10^{-6}, \quad (4)$$

between the GC and Earth. This constraint is at the

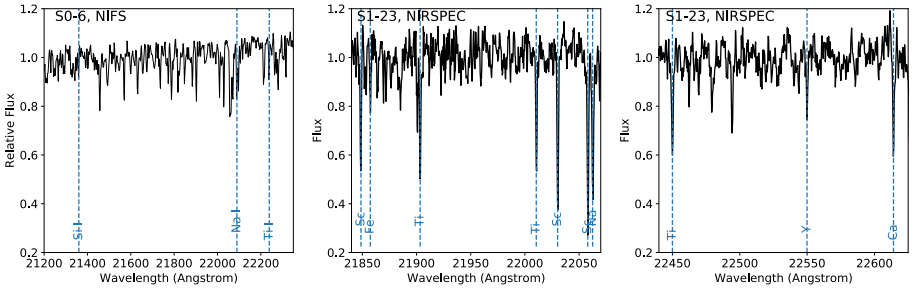

FIG. 3. Example spectra of the stars used in this work. **Left:** Spectrum of the star S0-6 observed using the NIFS spectrograph with a spectral resolution R = 5000. We have identified 3 lines that are suitable for the fine structure constant analysis. **Center & Right:** Spectra of the star S1-23 observed with the NIRSPEC instrument with R = 20,000. This higher spectral resolution allows us to identify 10 atomic lines for use in this experiment.

same level of magnitude as the ones obtained from quasar observations and is the first constraint on a possible variation of α around a BH.

In several alternative theories of gravitation, the fine structure constant becomes dependent on the gravitational potential (see e.g. [48]) and it is useful to consider the following parametrization

$$\frac{\Delta\alpha}{\alpha} = \beta_\alpha \frac{\Delta U}{c^2}\,, \tag{5}$$

where U is the Newtonian potential, c the speed of light in a vacuum and where β_α depends on the fundamental parameters of the theory. An estimate of the gravitational potential probed by the 5 stars considered in this analysis is required in order to constrain the β_α parameter. We infer the radial acceleration experienced by the stars using 25 years of astrometric measurements of the GC. Between 1995 and 2005, speckle imaging data provides astrometric diffraction-limited measurements of the central 5" × 5" of the GC [26, 28, 49]. Between 2005 and 2018, adaptive optics (AO) imaging provides high-resolution images of the central 10"× 10" of the GC [26, 28]. AO allows for more efficient observations at the diffraction limit, resulting in measurements typically one order of magnitude better than speckle observations. These astrometric measurements are aligned [50] in a common reference frame defined by tying infrared observations of seven SiO masers [51, 52] to their radio counterpart [53]. The resulting 2-D position measurements of the 5 stars considered in our analysis are provided in the Sec. III from the supplemental material [40]. A polynomial fit of these measurements give an estimate of the 3D radial acceleration of these stars which is transformed into an estimate of the gravitational potential using the the SMBH mass $M = 3.975 \times 10^6 M_\odot$ reported in [28]. The estimate of the gravitational potential experienced by each star is reported in Tab. II. A fit combining the measurements from the 5 stars and using the estimate from the gravitational potential from Tab. II leads to

$$\beta_\alpha = 3.6 \pm 12.0\,, \tag{6}$$

at 68% confidence level. No deviation from GR is reported. This result is 8 orders of magnitude less constraining than a similar constraint obtained with atomic clocks around the Sun [20] and one order of magnitude less constraining than a similar result obtained around a white dwarf [25]. Nevertheless, this is the first time such a measurement is performed around a BH and around such a massive object (see Fig. 1). Such a measurement is particularly appropriate to constrain the presence of a scalar field around a BH, which can naturally be enhanced in theories exhibiting BH scalarization mechanism, see e.g. [35, 54].

In conclusion, we propose a new method to search for a variation of the fine structure constant around a SMBH. Using existing measurements from NIFS spectrograph at GEMINI, from IRCS spectrograph from Subaru and from the NIRSPEC spectrograph at the Keck Observatory, we report a constraint on $\Delta\alpha/\alpha$ below 10^{-5} and a dependency of $\Delta\alpha/\alpha$ on the gravitational potential at the level of 10. This is the first time such a search has been performed around a compact object, around a BH or around such a massive object ($\sim 4 \times 10^6 M_\odot$), see Fig. 1. The results reported in this Letter could be improved by dedicated measurement sessions using high resolution spectrograph to measure spectrum of late-type stars closer to the GC. For example, a dedicated measurement of S0-6's spectrum using NIRSPEC could improve the limit on β_α by one order of magnitude. Furthermore, it is expected that future spectrographs with advanced AO systems such as KAPA at Keck [55] would be able to measure spectrum of fainter late-type stars that are orbiting close to the GC (like e.g. S0-38/S38 [26]), allowing us to improve significantly the current constraints (by up to 4 orders of magnitude) and allowing one to probe the fine structure constant in a higher gravitational potential. Finally, after the search for a fifth force [27, 32], the relativistic redshift measurement of the star S0-2/S2 [28, 30]

and a null test of the local position invariance using S0-2/S2 measurements [31], this analysis gives a new example of implications of GC measurements in term of fundamental physics.

Acknowledgments.

We thank the staff and astronomers at Keck Observatory and Gemini Observatory, especially Randy Campbell and Terry Stickel for all their help in obtaining the new NIRSPEC data. Some of the data presented herein were obtained at the W. M. Keck Observatory, which is operated as a scientific partnership among the California Institute of Technology, the University of California and the National Aeronautics and Space Administration and which was made possible by the generous financial support of the W. M. Keck Foundation. This work is partly based on observations obtained (Program ID GN-2018A-Q-123, PI: Do) at the Gemini Observatory, which is operated by the Association of Universities for Research in Astronomy, Inc., under a cooperative agreement with the NSF on behalf of the Gemini partnership: the National Science Foundation (United States), National Research Council (Canada), CONICYT (Chile), Ministerio de Ciencia, Tecnologia e Innovación Productiva (Argentina), Ministério da Ciencia, Tecnologia e Inovacao (Brazil), and Korea Astronomy and Space Science Institute (Republic of Korea). This work is also based in part on data collected at Subaru Telescope, which is operated by the National Astronomical Observatory of Japan. S. N. was supported by JSPS KAKENHI, Grants No. JP15K13463, No. JP18K18760, and No. JP19H00695. The authors wish to recognize that the summit of Maunakea has always held a very significant cultural role for the indigenous Hawaiian community. We are most fortunate to have the opportunity to observe from this mountain. Support for this work was provided by NSF AAG AST-1909554, the W.M. Keck Foundation, the Heising-Simons Foundation, and the Gordon and Betty Moore Foundation. Y. T. was supported by JSPS KAKENHI, Grant-in-Aid for Young Scientists (B) 26800150. We thank Julian Berengut for making the AMBiT software publicly available, and for discussions regarding its use.

[1] T. R. Taylor and G. Veneziano, Physics Letters B **213**, 450 (1988); T. Damour and A. M. Polyakov, Nuclear Physics B **423**, 532 (1994); General Relativity and Gravitation **26**, 1171 (1994).
[2] P. Fayet, Phys. Rev. D **97**, 055039 (2018); Phys. Rev. D **99**, 055043 (2019).
[3] I. Antoniadis, S. Dimopoulos, and G. Dvali, Nuclear Physics B **516**, 70 (1998); V. A. Rubakov, Physics Uspekhi **44**, 871 (2001); R. Maartens and K. Koyama, Living Reviews in Relativity **13**, 5 (2010); I. Antoniadis, S. Baessler, M. Büchner, V. V. Fedorov, S. Hoedl, A. Lambrecht, V. V. Nesvizhevsky, G. Pignol, K. V. Protasov, S. Reynaud, and Y. Sobolev, Comptes Rendus Physique **12**, 755 (2011).
[4] A. Arvanitaki, J. Huang, and K. Van Tilburg, Phys. Rev. D **91**, 015015 (2015); Y. V. Stadnik and V. V. Flambaum, Physical Review Letters **115**, 201301 (2015); A. Hees, O. Minazzoli, E. Savalle, Y. V. Stadnik, and P. Wolf, Phys. Rev. D **98**, 064051 (2018).
[5] S. M. Carroll, S. Mantry, M. J. Ramsey-Musolf, and C. W. Stubbs, Physical Review Letters **103**, 011301 (2009).
[6] J. Khoury and A. Weltman, Phys. Rev. Lett. **93**, 171104 (2004); Phys. Rev. D **69**, 044026 (2004).
[7] C. J. A. P. Martins, A. M. M. Pinho, R. F. C. Alves, M. Pino, C. I. S. A. Rocha, and M. von Wietersheim, J. Cosmology Astropart. Phys. **8**, 047 (2015); C. J. A. P. Martins and A. M. M. Pinho, Phys. Rev. D **91**, 103501 (2015).
[8] T. Damour, Classical and Quantum Gravity **29**, 184001 (2012).
[9] C. M. Will, Living Reviews in Relativity **17**, 4 (2014).
[10] J.-P. Uzan, Living Reviews in Relativity **14**, 2 (2011).
[11] H. Marion, F. Pereira Dos Santos, M. Abgrall, S. Zhang, Y. Sortais, S. Bize, I. Maksimovic, D. Calonico, J. Grünert, C. Mandache, P. Lemonde, G. Santarelli, P. Laurent, A. Clairon, and C. Salomon, Physical Review Letters **90**, 150801 (2003).
[12] S. Bize, S. A. Diddams, U. Tanaka, C. E. Tanner, W. H. Oskay, R. E. Drullinger, T. E. Parker, T. P. Heavner, S. R. Jefferts, L. Hollberg, W. M. Itano, and J. C. Bergquist, Physical Review Letters **90**, 150802 (2003).
[13] T. Rosenband, D. B. Hume, P. O. Schmidt, C. W. Chou, A. Brusch, L. Lorini, W. H. Oskay, R. E. Drullinger, T. M. Fortier, J. E. Stalnaker, S. A. Diddams, W. C. Swann, N. R. Newbury, W. M. Itano, D. J. Wineland, and J. C. Bergquist, Science **319**, 1808 (2008).
[14] J. Guéna, M. Abgrall, D. Rovera, P. Rosenbusch, M. E. Tobar, P. Laurent, A. Clairon, and S. Bize, Physical Review Letters **109**, 080801 (2012).
[15] M. E. Tobar, P. L. Stanwix, J. J. McFerran, J. Guéna, M. Abgrall, S. Bize, A. Clairon, P. Laurent, P. Rosenbusch, D. Rovera, and G. Santarelli, Phys. Rev. D **87**, 122004 (2013).
[16] N. Leefer, C. T. M. Weber, A. Cingöz, J. R. Torgerson, and D. Budker, Physical Review Letters **111**, 060801 (2013).
[17] R. M. Godun, P. B. R. Nisbet-Jones, J. M. Jones, S. A. King, L. A. M. Johnson, H. S. Margolis, K. Szymaniec, S. N. Lea, K. Bongs, and P. Gill, Physical Review Letters **113**, 210801 (2014).
[18] N. Huntemann, B. Lipphardt, C. Tamm, V. Gerginov, S. Weyers, and E. Peik, Physical Review Letters **113**, 210802 (2014).
[19] S. Peil, S. Crane, J. L. Hanssen, T. B. Swanson, and C. R. Ekstrom, Phys. Rev. A **87**, 010102 (2013).
[20] N. Ashby, T. E. Parker, and B. R. Patla, Nature Physics **14**, 822 (2018).
[21] K. Van Tilburg, N. Leefer, L. Bougas, and D. Budker, Physical Review Letters **115**, 011802 (2015); A. Hees, J. Guéna, M. Abgrall, S. Bize, and P. Wolf, Physical Review Letters **117**, 061301 (2016).
[22] J. K. Webb, V. V. Flambaum, C. W. Churchill, M. J. Drinkwater, and J. D. Barrow, Physical Review Let-

ters **82**, 884 (1999); J. K. Webb, M. T. Murphy, V. V. Flambaum, V. A. Dzuba, J. D. Barrow, C. W. Churchill, J. X. Prochaska, and A. M. Wolfe, Physical Review Letters **87**, 091301 (2001); M. T. Murphy, J. K. Webb, V. V. Flambaum, V. A. Dzuba, C. W. Churchill, J. X. Prochaska, J. D. Barrow, and A. M. Wolfe, MNRAS **327**, 1208 (2001); J. K. Webb, M. T. Murphy, V. V. Flambaum, and S. J. Curran, Ap&SS **283**, 565 (2003); M. T. Murphy, J. K. Webb, and V. V. Flambaum, MNRAS **345**, 609 (2003); R. Srianand, H. Chand, P. Petitjean, and B. Aracil, Physical Review Letters **92**, 121302 (2004); H. Chand, R. Srianand, P. Petitjean, and B. Aracil, A&A **417**, 853 (2004); P. Tzanavaris, J. K. Webb, M. T. Murphy, V. V. Flambaum, and S. J. Curran, Physical Review Letters **95**, 041301 (2005); P. Tzanavaris, M. T. Murphy, J. K. Webb, V. V. Flambaum, and S. J. Curran, MNRAS **374**, 634 (2007); M. T. Murphy, J. K. Webb, and V. V. Flambaum, MNRAS **384**, 1053 (2008); R. Srianand, P. Noterdaeme, C. Ledoux, and P. Petitjean, A&A **482**, L39 (2008); P. Petitjean, R. Srianand, H. Chand, A. Ivanchik, P. Noterdaeme, and N. Gupta, Space Sci. Rev. **148**, 289 (2009); J. K. Webb, J. A. King, M. T. Murphy, V. V. Flambaum, R. F. Carswell, and M. B. Bainbridge, Physical Review Letters **107**, 191101 (2011); J. A. King, J. K. Webb, M. T. Murphy, V. V. Flambaum, R. F. Carswell, M. B. Bainbridge, M. R. Wilczynska, and F. E. Koch, MNRAS **422**, 3370 (2012).

[23] Planck Collaboration, P. A. R. Ade, and et. al., A&A **571**, A16 (2014), arXiv:1303.5076 [astro-ph.CO].

[24] P. P. Avelino, S. Esposito, G. Mangano, C. J. A. P. Martins, A. Melchiorri, G. Miele, O. Pisanti, G. Rocha, and P. T. P. Viana, Phys. Rev. D **64**, 103505 (2001).

[25] J. C. Berengut, V. V. Flambaum, A. Ong, J. K. Webb, J. D. Barrow, M. A. Barstow, S. P. Preval, and J. B. Holberg, Physical Review Letters **111**, 010801 (2013).

[26] A. M. Ghez, B. L. Klein, M. Morris, and E. E. Becklin, ApJ **509**, 678 (1998); A. M. Ghez, M. Morris, E. E. Becklin, A. Tanner, and T. Kremenek, Nature **407**, 349 (2000); A. M. Ghez, G. Duchêne, K. Matthews, S. D. Hornstein, A. Tanner, J. Larkin, M. Morris, E. E. Becklin, S. Salim, T. Kremenek, D. Thompson, B. T. Soifer, G. Neugebauer, and I. McLean, ApJ **586**, L127 (2003); A. M. Ghez, S. Salim, S. D. Hornstein, A. Tanner, J. R. Lu, M. Morris, E. E. Becklin, and G. Duchêne, ApJ **620**, 744 (2005); A. M. Ghez, S. D. Hornstein, J. R. Lu, A. Bouchez, D. Le Mignant, M. A. van Dam, P. Wizinowich, K. Matthews, M. Morris, E. E. Becklin, R. D. Campbell, J. C. Y. Chin, S. K. Hartman, E. M. Johansson, R. E. Lafon, P. J. Stomski, and D. M. Summers, ApJ **635**, 1087 (2005); A. M. Ghez, S. Salim, N. N. Weinberg, J. R. Lu, T. Do, J. K. Dunn, K. Matthews, M. R. Morris, S. Yelda, E. E. Becklin, T. Kremenek, M. Milosavljevic, and J. Naiman, ApJ **689**, 1044 (2008); L. Meyer, A. M. Ghez, R. Schödel, S. Yelda, A. Boehle, J. R. Lu, T. Do, M. R. Morris, E. E. Becklin, and K. Matthews, Science **338**, 84 (2012); A. Boehle, A. M. Ghez, R. Schödel, L. Meyer, S. Yelda, S. Albers, G. D. Martinez, E. E. Becklin, T. Do, J. R. Lu, K. Matthews, M. R. Morris, B. Sitarski, and G. Witzel, ApJ **830**, 17 (2016); D. S. Chu, T. Do, A. Hees, A. Ghez, S. Naoz, G. Witzel, S. Sakai, S. Chappell, A. K. Gautam, J. R. Lu, and K. Matthews, ApJ **854**, 12 (2018).

[27] A. Hees, T. Do, A. M. Ghez, G. D. Martinez, S. Naoz, E. E. Becklin, A. Boehle, S. Chappell, D. Chu, A. Dehghanfar, K. Kosmo, J. R. Lu, K. Matthews, M. R. Morris, S. Sakai, R. Schödel, and G. Witzel, Physical Review Letters **118**, 211101 (2017).

[28] T. Do, A. Hees, A. Ghez, G. D. Martinez, D. S. Chu, S. Jia, S. Sakai, J. R. Lu, A. K. Gautam, K. K. O'Neil, E. E. Becklin, M. R. Morris, K. Matthews, S. Nishiyama, R. Campbell, S. Chappell, Z. Chen, A. Ciurlo, A. Dehghanfar, E. Gallego-Cano, W. E. Kerzendorf, J. E. Lyke, S. Naoz, H. Saida, R. Schödel, M. Takahashi, Y. Takamori, G. Witzel, and P. Wizinowich, Science **365**, 664 (2019).

[29] R. Genzel, A. Eckart, T. Ott, and F. Eisenhauer, MNRAS **291**, 219 (1997); A. Eckart and R. Genzel, MNRAS **284**, 576 (1997); R. Schödel, T. Ott, R. Genzel, R. Hofmann, M. Lehnert, A. Eckart, N. Mouawad, T. Alexander, M. J. Reid, R. Lenzen, M. Hartung, F. Lacombe, D. Rouan, E. Gendron, G. Rousset, A.-M. Lagrange, W. Brandner, N. Ageorges, C. Lidman, A. F. M. Moorwood, J. Spyromilio, N. Hubin, and K. M. Menten, Nature **419**, 694 (2002); A. Eckart, R. Genzel, T. Ott, and R. Schödel, **331**, 917 (2002); F. Eisenhauer, R. Schödel, R. Genzel, T. Ott, M. Tecza, R. Abuter, A. Eckart, and T. Alexander, ApJ **597**, L121 (2003); F. Eisenhauer, R. Genzel, T. Alexander, R. Abuter, T. Paumard, T. Ott, A. Gilbert, S. Gillessen, M. Horrobin, S. Trippe, H. Bonnet, C. Dumas, N. Hubin, A. Kaufer, M. Kissler-Patig, G. Monnet, S. Ströbele, T. Szeifert, A. Eckart, R. Schödel, and S. Zucker, ApJ **628**, 246 (2005); S. Gillessen, F. Eisenhauer, T. K. Fritz, H. Bartko, K. Dodds-Eden, O. Pfuhl, T. Ott, and R. Genzel, ApJ **707**, L114 (2009); S. Gillessen, F. Eisenhauer, S. Trippe, T. Alexander, R. Genzel, F. Martins, and T. Ott, ApJ **692**, 1075 (2009); S. Gillessen, P. M. Plewa, F. Eisenhauer, R. Sari, I. Waisberg, M. Habibi, O. Pfuhl, E. George, J. Dexter, S. von Fellenberg, T. Ott, and R. Genzel, ApJ **837**, 30 (2017); Gravity Collaboration, R. Abuter, and et.al., A&A **625**, L10 (2019).

[30] Gravity Collaboration, R. Abuter, and et.al., A&A **615**, L15 (2018).

[31] Gravity Collaboration, R. Abuter, and et.al., Physical Review Letters **122**, 101102 (2019).

[32] D. Borka, P. Jovanović, V. Borka Jovanović, and A. F. Zakharov, J. Cosmology Astropart. Phys. **11**, 050 (2013); A. F. Zakharov, P. Jovanović, D. Borka, and V. Borka Jovanović, J. Cosmology Astropart. Phys. **05**, 045 (2016); J. Cosmology Astropart. Phys. **4**, 050 (2018).

[33] K. Hinterbichler and J. Khoury, Physical Review Letters **104**, 231301 (2010); K. Hinterbichler, J. Khoury, A. Levy, and A. Matas, Phys. Rev. D **84**, 103521 (2011).

[34] A. I. Vainshtein, Physics Letters B **39**, 393 (1972); C. Deffayet, G. Dvali, G. Gabadadze, and A. Vainshtein, Phys. Rev. D **65**, 044026 (2002).

[35] D. D. Doneva and S. S. Yazadjiev, Physical Review Letters **120**, 131103 (2018); G. Antoniou, A. Bakopoulos, and P. Kanti, Physical Review Letters **120**, 131102 (2018); H. O. Silva, J. Sakstein, L. Gualtieri, T. P. Sotiriou, and E. Berti, Physical Review Letters **120**, 131104 (2018).

[36] T. Do, J. R. Lu, A. M. Ghez, M. R. Morris, S. Yelda, G. D. Martinez, S. A. Wright, and K. Matthews, ApJ **764**, 154 (2013), arXiv:1301.0539 [astro-ph.SR].

[37] S. Nishiyama, H. Saida, Y. Takamori, M. Takahashi, R. Schödel, F. Najarro, S. Hamano, M. Omiya,

M. Tamura, M. Takahashi, H. Gorin, S. Nagatomo, and T. Nagata, PASJ **70**, 74 (2018), arXiv:1709.01598 [astro-ph.GA].
[38] H. Saida, S. Nishiyama, T. Ohgami, Y. Takamori, M. Takahashi, Y. Minowa, F. Najarro, S. Hamano, M. Omiya, A. Iwamatsu, M. Takahashi, H. Gorin, T. Kara, A. Koyama, Y. Ohashi, M. Tamura, S. Nagatomo, T. Zenko, and T. Nagata, PASJ **71** (2019), 10.1093/pasj/psz111, 126, arXiv:1910.02632 [gr-qc].
[39] T. Do, W. Kerzendorf, Q. Konopacky, J. M. Marcinik, A. Ghez, J. R. Lu, and M. R. Morris, ApJ **855**, L5 (2018), arXiv:1802.08270 [astro-ph.GA].
[40] See Supplemental Material available on-line from the web site from Phys. Rev. Letters.
[41] V. A. Dzuba, V. V. Flambaum, and M. G. Kozlov, Phys. Rev. A **54**, 3948 (1996); V. A. Dzuba and W. R. Johnson, Phys. Rev. A **57**, 2459 (1998).
[42] J. C. Berengut, Phys. Rev. A **94**, 012502 (2016).
[43] V. A. Dzuba, J. C. Berengut, C. Harabati, and V. V. Flambaum, Phys. Rev. A **95**, 012503 (2017).
[44] A. J. Geddes, L. V. Skripnikov, A. Borschevsky, J. C. Berengut, V. V. Flambaum, and T. P. Rakitzis, Phys. Rev. A **98**, 022508 (2018).
[45] E. V. Kahl and J. C. Berengut, Computer Physics Communications **238**, 232 (2019).
[46] A. Kramida, Y. Ralchenko, J. Reader, and The NIST ASD Team (2018), NIST Atomic Spectra Database (ver. 5.6.1) **[Online]**, http://physics.nist.gov/asd (2019).
[47] F. Feroz and M. P. Hobson, MNRAS **384**, 449 (2008); F. Feroz, M. P. Hobson, and M. Bridges, MNRAS **398**, 1601 (2009).
[48] J. D. Bekenstein, Phys. Rev. D **25**, 1527 (1982); H. B. Sandvik, J. D. Barrow, and J. Magueijo, Physical Review Letters **88**, 031302 (2002); A. Hees and O. Minazzoli, arXiv e-prints (2015), arXiv:1512.05233 [gr-qc].
[49] Z. Chen, E. Gallego-Cano, T. Do, G. Witzel, A. M. Ghez, R. Schödel, B. N. Sitarski, E. E. Becklin, J. Lu, M. R. Morris, A. Dehghanfar, A. K. Gautam, A. Hees, M. W. Hosek, Jr., S. Jia, A. C. Mangian, and K. Matthews, ApJ **882**, L28 (2019).
[50] S. Jia, J. R. Lu, S. Sakai, A. K. Gautam, T. Do, M. W. Hosek, Jr., M. Service, A. M. Ghez, E. Gallego-Cano, R. Schödel, A. Hees, M. R. Morris, E. Becklin, and K. Matthews, ApJ **873**, 9 (2019).
[51] S. Yelda, J. R. Lu, A. M. Ghez, W. Clarkson, J. Anderson, T. Do, and K. Matthews, ApJ **725**, 331-352 (2010); S. Yelda, L. Meyer, A. Ghez, and T. Do, in *Proceedings of the Third AO4ELT Conference*, edited by S. Esposito and L. Fini (2013) p. 83.
[52] S. Sakai, J. R. Lu, A. Ghez, S. Jia, T. Do, G. Witzel, A. K. Gautam, A. Hees, E. Becklin, K. Matthews, and M. W. Hosek, Jr., ApJ **873**, 65 (2019).
[53] M. J. Reid, K. M. Menten, S. Trippe, T. Ott, and R. Genzel, ApJ **659**, 378 (2007).
[54] A. Hees, O. Minazzoli, E. Savalle, Y. V. Stadnik, P. Wolf, and B. M. Roberts, in *Proceedings of the 52nd Rencontres de Moriond - Gravitation session* (2019).
[55] P. Wizinowich, J. Chin, K. Casey, S. Cetre, C. Correia, L. Hunter, S. Lilley, J. Lu, S. Ragland, E. Wetherell, A. Ghez, T. Do, T. Jones, M. Liu, D. Mawet, C. Max, M. Morris, T. Treu, and T. Wright, in *Proceedings of the Sixth AO4ELT Conference* (2019).
[56] J. C. Berengut, V. A. Dzuba, V. V. Flambaum, and A. Ong, Physical Review Letters **109**, 070802 (2012).
[57] M. S. Safronova, Annalen der Physik **0**, 1800364 (2019).
[58] M. G. Kozlov and D. Budker, Annalen der Physik , 1800254 (2018).
[59] V. A. Dzuba, V. V. Flambaum, and M. G. Kozlov, Phys. Rev. A **99**, 032501 (2019).
[60] B. G. C. Lackenby, V. A. Dzuba, and V. V. Flambaum, Phys. Rev. A **99**, 042509 (2019), arXiv:1902.06819 [physics.atom-ph].
[61] J. C. Berengut, V. V. Flambaum, and M. G. Kozlov, Phys. Rev. A **73**, 012504 (2006).
[62] J. C. Berengut, V. V. Flambaum, and M. G. Kozlov, Journal of Physics B Atomic Molecular Physics **41**, 235702 (2008).
[63] V. A. Dzuba, Phys. Rev. A **71**, 032512 (2005).
[64] V. V. Flambaum and V. A. Dzuba, Canadian Journal of Physics **87**, 25 (2009).
[65] V. A. Dzuba and V. V. Flambaum, Phys. Rev. A **77**, 012515 (2008).
[66] V. A. Dzuba, V. V. Flambaum, P. G. Silvestrov, and O. P. Sushkov, Journal of Physics B Atomic Molecular Physics **20**, 1399 (1987).
[67] V. A. Dzuba, V. V. Flambaum, and O. P. Sushkov, Physics Letters A **140**, 493 (1989).
[68] J. C. Berengut, V. A. Dzuba, V. V. Flambaum, and M. V. Marchenko, Phys. Rev. A **70**, 064101 (2004).

Appendix A: Computation of the sensitivity of the transition energies to the fine structure constant

The atomic transition frequency can be expressed as

$$\omega = \omega_0 + qx, \tag{A1}$$

where ω_0 is the nominal (observed laboratory) transition frequency, x parameterizes the variation in α:

$$x \equiv (\alpha/\alpha_0)^2 - 1, \tag{A2}$$

and q is the sensitivity factor. Assuming the variation in α is small, q can be determined from the derivative of ω to first-order around $x = 0$. In practice, this is done by calculating the relevant transition transition frequencies and explicitly allowing the value for α to vary inside the code (i.e., choosing small, non-zero values for x, denoted $\pm\delta x$). Then, we have

$$q = \left.\frac{d\omega}{dx}\right|_{x=0} \approx \frac{\omega(+\delta x) - \omega(-\delta x)}{2\delta x}. \tag{A3}$$

We take values between $\delta x = 0.05$ and 0.1. Multiple values are used to check for non-linearities. Note that none of the atomic systems considered here have particularly high sensitivities (large q values), so no non-linear effects are expected, and indeed none are observed. Much larger sensitivities can be found, e.g., in highly charged ions with large nuclear charges [56, 57]. In general, δx must be taken small enough so that the linear requirement of (A3) is valid, but must also be large enough for the variation $\delta\omega$ to avoid numerical errors.

Note that q has energy units. It is convenient to further define a dimensionless sensitivity factor, k_α, defined via

$$\frac{\delta\omega}{\omega_0} = k_\alpha \frac{\delta\alpha}{\alpha}, \tag{A4}$$

which is linked to q as

$$k_\alpha = 2q/\omega_0\,. \tag{A5}$$

For the infra-red transitions considered in this work, ω_0 is small compared to optical transitions from the ground state. This manifests as an apparent enhancement in the magnitude of k; however, we note that this is partly compensated for by the uncertainty in the measurement of the observed frequencies (see also discussion in Ref. [58]).

1. Method for calculation

We use a method that is based on the combination of the configuration interaction (CI) method with many-body perturbation theory (MBPT) [41]. The CI method accurately takes into account the valence–valence electron correlations, while the inclusion of MBPT allows an accurate treatment of the core–valence correlations. The specific method we employ was developed in Ref. [45], see also Refs. [42–44]. This implementation allows systems with a large number of valence electrons to be calculated accurately with reasonable computational resources. Other CI methods for large valence systems have also proved successful [59, 60].

The details of the method are presented in the above references, here we just give a brief overview. The effective Hamiltonian for system of M valence electrons is written as

$$\hat{H} = \sum_i^M \hat{h}_1(\boldsymbol{r}_i) + \sum_{i<j}^M \hat{h}_2(\boldsymbol{r}_i, \boldsymbol{r}_j), \tag{A6}$$

where $\hat{h}_1$ is the single-electron part of the Dirac Hamiltonian (in atomic units, $e = m_e = \hbar = 1$),

$$\hat{h}_1 = c\gamma^0\boldsymbol{\gamma}\cdot\hat{\boldsymbol{p}} + c^2(\gamma^0 - 1) - V^{\text{nuc.}} + V^{N-M} + \hat{\Sigma}_1, \tag{A7}$$

and $\hat{h}_2$ is the two-electron part,

$$\hat{h}_2 = \frac{1}{|\boldsymbol{r}_i - \boldsymbol{r}_j|} + \hat{\Sigma}_2. \tag{A8}$$

In the above equations, $\boldsymbol{\gamma}$ and γ^0 are Dirac matrices, $c = 1/\alpha$ is the speed of light, $V^{\text{nuc.}} \approx Z/r$ is the nuclear potential (formed assuming a Fermi-type nuclear distribution), and V^{N-M} is the Hartree-Fock core potential, formed from the $N - M$ core electrons (N is the total number of electrons).

The $\hat{\Sigma}$ terms are the correlation potentials, calculated to the second order in perturbation theory, without which the above equations would correspond to the conventional CI method. The single electron correlation potential $\hat{\Sigma}_1$ represents the interaction of a single valence electron with the atomic core, and $\hat{\Sigma}_2$, a two-electron operator, represents the screening of the valence-valence Coulomb interaction by the core electrons (see Refs. [41, 43, 61] for details). Effective three-body MBPT contributions as introduced in Ref. [62] are also included. For the systems considered here they make a reasonably small contribution, but do improve the accuracy.

The M-body CI wavefunctions are expanded as linear combinations of sets of M-body configuration functions (Slater determinants) that conserve a given J_z-parity symmetry,

$$|\psi_{J_z^\pi}\rangle = \sum_a c_a |a,\, J_z^\pi\rangle \tag{A9}$$

The c expansion coefficients and CI energies are then found from the CI matrix eigenvalue problem

$$\sum_a \Big(\langle a|\hat{H}|b\rangle - E\delta_{ab}\Big)\, c_a = 0. \tag{A10}$$

Many of the non-diagonal terms in the above matrix contribute negligibly. In the "emu CI" approach [45], some of these terms can be neglected from the calculations, which greatly reduces the number of integrals that need to be calculated and stored for the CI matrix.

The configuration functions are themselves formed from a set of single-particle basis orbitals, ϕ. These orbitals (which are also used to calculate the MBPT diagrams) are constructed using a potential that is formed by solving the Hartree-Fock equations self-consistently for a subset of the atomic orbitals. In theory, with a complete enough basis, if all MBPT diagrams are calculated and the CI procedure converges, the choice of potential doesn't matter. In practice, both the CI and MBPT parts are calculated approximately using a finite basis, and the choice of potential has a significant impact on the convergence of the calculations. One common choice is to use the same V^{N-M} potential as in Eq. (A7), where the HF equations are solved for the closed-shell core electrons excluding all valence electrons. Another is the V^{N-1} potential, which corresponds to solving the HF equations including all but one of the electrons, and in general will involve partially-filled open shells.

The V^{N-M} potential is convenient for evaluating the MBPT diagrams [63], while V^{N-1} potential has the advantage of producing more realistic orbitals, allowing the CI expansion to converge more quickly. Many of the states considered in this work lie relatively high in the spectrum. In this regime, the core-valence correlation effects become less important, and the accuracy is mainly controlled the convergence of the CI part of the problem. We use the V^{N-M} potential for the two valence electron systems (Ca). For the other systems with more valence electrons, we use the V^{N-1} potential which allows faster convergence of CI. Calculations including q factors for some of the lower-lying states of Ca were presented

in Ref. [64], and our calculations are in good agreement with those.

We treat silicon ($3s^2 3p^2$, $^3P_0$ ground state) as a two valence system, with the $3s^2$ orbitals remaining in the core. We then allow single and double hole excitations into this $3s$ sub-shell, using the particle-hole formalism described in Ref. [42]. Note that the sign of the r_{ij}^{-1} term in Eq. (A8) becomes negative for electron-hole interactions. The affect of this is that some of the configuration functions are two-body, while others are four and six-body functions. Since the configurations that include the $3s^2$ shell intact dominate the CI expansion, this method allows a significant reduction in the size of the CI matrix, while not neglecting the excitations of the $3s$ orbitals, which are nonetheless important.

For iron ($3d^6 4s^2\ ^5D_4$ ground state), which has 8 valence electrons, we employ a restricted version of the method. We use the V^{N-1} potential, and allow only single excitations from specific reference configurations relevant to this work ($3d^6 4s^2$ for the even states, and $3d^6 4s 4p$ for the odd states). We treat the $4s^2$ shell as though it were in the core, and allow single hole excitations into this shell. Further, we do not include MBPT corrections (core–valence electron correlations). This is a reasonable approximation, since the valence–valence electron correlations (treated at the CI level) dominate for systems with a large number of valence electrons. Some calculations for iron, including for the q sensitivities were presented in Ref. [65], though not for the particular states of interest for this work. We find that the q factors are rather sensitive to configuration mixing; the same conclusion was found in Ref. [65]. However, we find quite good agreement with experimental energies, and reasonable agreement between the q values found in this work and those of Ref. [65] (our q values are systematically around $\sim$20–30% larger). Conservatively, we assume a large 40% uncertainty for all iron q values, taking into account the spread of calculated q values using different CI basis expansions.

We use a different approach for sodium, which has a single valence electron above a closed-shell core. Namely, we employ the correlation potential method [66], in which the single-particle correlation potential is included into the Hartree-Fock equations

$$\left(\hat{h}^{\rm HF} + \hat{\Sigma}_1\right)\phi_a = \varepsilon_a \phi_a, \tag{A11}$$

which are solved self-consistently for each of the relevant valence orbitals (which, when calculated this way, are known as Brueckner orbitals). This is the same Hamiltonian as in Eq. (A7); note that $V^{N-M} = V^{N-1}$ for $M = 1$. Again, the correlation potential is calculated to second-order in perturbation theory, though we note that it is possible to significantly improve the accuracy by using an all-order method [67]. Including Σ into the self-consistent Hartree-Fock equations in this way effectively includes some classes of diagrams to all-orders [66]. Calculations of q-factors for the $3p$ and $4p$ states of sodium (referenced to the $3s$ ground state) were calculated in Ref. [68], using the same method employed here. In this work, we are interesting in transitions involving the $4s$ state.

2. Uncertainty in q

We estimate the uncertainty in each q value by taking into account both the errors in the energy-level determination, and the spread (stability) of the q values as calculated with differing approximations (for example, by using a smaller basis for CI). In most cases, the q values for each level are found to be rather stable, and can be calculated with relatively high accuracy ($\sim$ 1–10%). The uncertainty in the q values for the transitions of interest to this work, however, can be significantly larger. This is because we consider transitions between states that are relatively high in the spectrum, and have similar q values (leading to cancellation errors).

3. Results

Calculations of the energy levels, Landé g-factors, and $\delta\alpha$ sensitivity q-factors are shown for Y, Fe, Ti, Sc, Ca, Si, and Na in tables III through X. The q values are calculated with respect to the ground state. The g-factors are useful for identifying states. We don't present calculated g-factors for the lighter elements ($Z \leq 20$), since they do not vary significantly from the non-relativistic values. Table XI shows the q and k sensitivities for the specific transitions of interest for this work.

TABLE III. **Yttrium ($Z = 39$).** Comparison of experimental and calculated excitation energies ($\Delta E \equiv E_{\text{Calc.}} - E_{\text{Exp.}}$), with calculated Landé g-factors, and $\delta\alpha$ sensitivity q-factors (relative to the ground state). Levels involved in transitions studied in this work are shown in bold.

Leading		Energy (cm^{-1})			Landé g		
config.	Term	Exp.[46]	Calc.	ΔE	Exp.[46]	Calc.	q (cm^{-1})
Even Levels							
$4d^2 5s$	$^2D_{3/2}$	0	0		0.80	0.80	
$4d^2 5s$	$^2D_{5/2}$	530	581	50	1.20	1.20	530 (70)
$4d^2 5s$	$^4F_{3/2}$	10937	10778	−159	0.40	0.40	2880 (100)
$4d^2 5s$	$^4F_{5/2}$	11079	10935	−144	1.03	1.03	3030 (110)
$4d^2 5s$	$^4F_{7/2}$	**11278**	**11155**	**−123**	**1.24**	**1.24**	**3230 (120)**
$4d^2 5s$	$^4P_{1/2}$	15222	15426	204	2.61	2.66	2450 (260)
$4d^2 5s$	$^2F_{5/2}$	15327	15585	259	1.15	1.21	3740 (580)
$4d^2 5s$	$^4P_{3/2}$	15329	15544	215	1.62	1.72	2590 (250)
$4d^2 5s$	$^4P_{5/2}$	15477	15722	245	1.27	1.22	2230 (240)
$4d^2 5s$	$^2F_{7/2}$	15864	16176	312	1.17	1.14	3830 (170)
$4d^2 5s$	$^2D_{3/2}$	15994	16436	442	0.86	0.82	2890 (180)
$4d^2 5s$	$^2G_{7/2}$	18512	19176	664	0.90	0.89	3100 (180)
$4d^2 5s$	$^2P_{1/2}$	19238	19563	326		0.67	3400 (150)
$4d^2 5s$	$^2S_{1/2}$	23465	23924	459		2.00	1660 (300)
$4d^3$	$^4F_{7/2}$	29614	29468	−146		1.24	5490 (260)
$5s26s$	$^2S_{1/2}$	31672	31330	−342	2.03	2.01	−2720 (170)
Odd Levels							
$5s^2 5p$	$^2P^o_{1/2}$	10529	10174	−356	0.63	0.67	−2610 (100)
$5s^2 5p$	$^2P^o_{3/2}$	11360	11028	−331	1.34	1.33	−1710 (50)
$4d5s5p$	$^4F^o_{3/2}$	14949	14733	−216	0.47	0.44	480 (10)
$4d5s5p$	$^4F^o_{5/2}$	15246	15044	−202	1.08	1.05	770 (20)
$4d5s5p$	$^4F^o_{7/2}$	**15713**	**15556**	**−156**	**1.26**	**1.24**	**1280 (40)**
$4d5s5p$	$^2D^o_{5/2}$	16066	15835	−231	1.20	1.19	1610 (40)
$4d5s5p$	$^2D^o_{3/2}$	16146	15921	−226	0.80	0.79	1670 (50)
$4d5s5p$	$^4D^o_{1/2}$	16436	16155	−281	0.01	0.00	1190 (20)
$4d5s5p$	$^4D^o_{3/2}$	16597	16334	−263	1.22	1.17	1410 (30)
$4d5s5p$	$^4D^o_{5/2}$	16817	16567	−249	1.38	1.37	1590 (30)
$4d5s5p$	$^4D^o_{7/2}$	17116	16888	−228	1.42	1.43	1900 (50)
$4d5s5p$	$^4P^o_{1/2}$	18976	18815	−161		2.66	1390 (30)
$4d5s5p$	$^4P^o_{5/2}$	19148	19029	−119	1.49	1.59	1600 (50)
$4d5s5p$	$^2F^o_{7/2}$	21915	21893	−23	1.15	1.14	2450 (60)
$4d5s5p$	$^2P^o_{1/2}$	24699	24617	−81	0.67	0.67	2260 (70)
$4d5s5p$	$^2F^o_{7/2}$	24900	24822	−78	1.15	1.14	2150 (120)

TABLE IV. **Iron ($Z = 22$), even states.** Comparison of experimental and calculated excitation energies, with calculated Landé g-factors, and $\delta\alpha$ sensitivity q-factors for some of the lower odd states of iron. We estimate a $\sim$40% uncertainty for the q values.

	Energy (cm^{-1})				Landé g		
State	Exp.[46]	Calc.	Δ	Other [65]	Exp.[46]	Calc.	q (cm^{-1})
Leading configuration: $3d^6 4s^2$ ($J = 2$)							
$^5D_2$	704	803	-99	790	1.500	1.499	710
$^3P_2$	18378	19709	-1331		1.506	1.490	204
$^3F_2$	21039	23960	-2921		0.663	0.709	587
Leading configuration: $3d^7 4s$ ($J = 2$)							
$^5F_2$	7986	6592	1394	8078	1.000	1.000	2861
$^3F_2$	12969	14790	-1821	14171	0.670	0.694	2960
$^5P_2$	17727	15979	1748		1.820	1.813	2269
$^3P_2$	22838	23540	-702		1.498	1.354	1851
$^3P_2$	24336	25775	-1440		1.484	1.277	2609
$^3D_2$	26624	26836	-212		1.178	1.408	1677
$^1D_2$	28605	28513	92		1.028	1.073	1957
$^3F_2$	36941	36385	555			0.687	1922
Leading configuration: $3d^6 4s^2$ ($J = 3$)							
$^5D_3$	416	429	-13	464	1.500	1.499	396
$^3F_3$	20874	22709	-1835		1.073	1.061	246
$^3G_3$	24339	26316	-1977		0.761	0.783	1001
$^3D_3$	**29372**	**31928**	**-2556**		**1.326**	**1.327**	**312**
Leading configuration: $3d^7 4s$ ($J = 3$)							
$^5F_3$	7728	5404	2324	7779	1.250	1.247	2577
$^3F_3$	12561	12996	-435	13702	1.086	1.072	2662
$^5P_3$	17550	16785	765		1.666	1.654	2069
$^3G_3$	22249	20728	1522		0.756	0.767	2498
$^3D_3$	26225	24808	1417		1.335	1.332	1664
Leading configuration: $3d^6 4s^2$ ($J = 4$)							
$^5D_4$	0	0			1.500	1.499	
$^3H_4$	19788	19666	123		0.811	0.828	442
$^3F_4$	20641	22425	-1784		1.235	1.144	438
$^3G_4$	24119	26316	-2197		1.048	1.053	1734
$^1G_4$	29799	31893	-2094		0.979	1.001	499
Leading configuration: $3d^7 4s$ ($J = 4$)							
$^5F_4$	7377	4377	3000		1.350	1.346	2182
$^3F_4$	11976	12760	-784		1.254	1.247	2020
$^3G_4$	21999	19145	2855		1.051	1.017	1951
$^1G_4$	24575	22943	1631		1.001	0.978	2902

TABLE V. **Iron ($Z = 22$), odd states.** Comparison of experimental and calculated excitation energies, with calculated Landé g-factors, and $\delta\alpha$ sensitivity q-factors for some of the lower odd states of iron. We estimate a $\sim$40% uncertainty for the q values.

	Energy (cm^{-1})				Landé g		q (cm^{-1})	
State	Exp.[46]	Calc.	Δ	Other [65]	Exp.[46]	Calc.	Calc.	Other [65]
Leading configuration: $3d^6 4s4p$ ($J = 1$)								
$^7D^o_1$	20020	19855	165	19921	2.999	2.992	1568	1237
$^7F^o_1$	23245	22711	534	22338	1.549	1.505	1530	1227
$^5D^o_1$	26479	25364	1115	27094	1.495	1.480	2323	1616
$^5F^o_1$	27666	26774	893	28213	-0.012	0.023	2426	1680
$^5P^o_1$	29733	29378	355	30118	2.487	2.494	1879	1594
$^3D^o_1$	31937	31495	442	32750	0.513	0.559	2568	2119
$^3P^o_1$	34363	34565	-202		1.496	1.496	2014	
$^5P^o_1$	37410	36116	1293		2.502	2.493	903	
Leading configuration: $3d^6 4s4p$ ($J = 2$)								
$^7D^o_2$	19912	19568	345	19793	2.008	1.995	1445	1092
$^7F^o_2$	23193	22628	564	22282	1.504	1.505	1504	1184
$^7P^o_2$	24507	23859	648	23440	2.333	2.329	1539	1316
$^5D^o_2$	26340	24955	1385	26924	1.503	1.480	2284	1450
$^5F^o_2$	27560	26298	1262	28119	1.004	1.018	2421	1568
$^5P^o_2$	29469	29019	450	29795	1.835	1.827	1620	1310
$^3D^o_2$	31686	30817	869	32464	1.168	1.177	2647	1843
$^3F^o_2$	32134	31492	642	33263	0.682	0.751	2624	2177
$^3P^o_2$	**33947**	**34144**	**-197**		**1.493**	**1.494**	**1596**	
Leading configuration: $3d^6 4s4p$ ($J = 3$)								
$^7D^o_3$	19757	19243	514	19611	1.746	1.747	1267	891
$^7F^o_3$	23111	22468	643	22189	1.513	1.505	1436	1103
$^7P^o_3$	24181	23466	715	23034	1.908	1.910	1235	983
$^5D^o_3$	26140	24436	1704	26679	1.500	1.488	2122	1223
$^5F^o_3$	27395	25626	1769	27947	1.250	1.259	2370	1402
$^5P^o_3$	29056	28717	339	29340	1.657	1.661	1199	859
$^3D^o_3$	31323	30457	865	32032	1.321	1.324	2196	1456
$^3F^o_3$	31805	30787	1018	32883	1.086	1.071	2678	1808
Leading configuration: $3d^6 4s4p$ ($J = 4$)								
$^7D^o_4$	19562	18933	630	19390	1.642	1.649	1081	662
$^7F^o_4$	22997	22218	779	22062	1.493	1.507	1301	982
$^7P^o_4$	23711	22986	726	22543	1.747	1.739	778	491
$^5D^o_4$	25900	24081	1819	26428	1.502	1.500	1715	999
$^5F^o_4$	27167	24999	2167	27702	1.355	1.350	2183	1180
$^3F^o_4$	31307	29214	2093	32356	1.250	1.329	2342	1267

TABLE VI. **Titanium ($Z = 22$).** Comparison of experimental and calculated excitation energies, with calculated Landé g-factors, and $\delta\alpha$ sensitivity q-factors.

Leading config.	Term	Energy (cm^{-1}) Exp.[46]	Energy (cm^{-1}) Calc.	ΔE	Landé g Exp.[46]	Landé g Calc.	q (cm^{-1})
Even Levels							
$3d^2 4s2$	$^3F_2$	0	0		0.67	0.67	0
$3d^2 4s2$	$^3F_3$	170	233	63	1.08	1.08	220 (80)
$3d^3 4s$	$^5F_1$	6557	7800	1243	0.00	0.00	1280 (250)
$3d^3 4s$	$^5F_2$	6599	7849	1250	1.00	0.99	1330 (260)
$3d^3 4s$	$^5F_3$	6661	7929	1268	1.25	1.25	1410 (270)
$3d^2 4s2$	$^1D_2$	7255	8486	1230	1.02	1.02	130 (40)
$3d^2 4s2$	$^3P_0$	8437	9264	828			90 (40)
$3d^2 4s2$	$^3P_1$	8492	9316	824	1.50	1.50	160 (40)
$3d^2 4s2$	$^3P_2$	8602	9509	906	1.48	1.49	350 (60)
$3d^3 4s$	$^3F_2$	11532	13812	2280	0.67	0.67	1520 (310)
$3d^3 4s$	$^3F_3$	11640	13963	2323	1.08	1.08	1650 (340)
$3d^3 4s$	$^5P_1$	**13982**	**16145**	**2163**	**2.50**	**2.50**	**1290 (210)**
$3d^3 4s$	$^5P_2$	**14028**	**16214**	**2186**	**1.83**	**1.82**	**1340 (220)**
$3d^3 4s$	$^5P_3$	14106	16328	2223	1.67	1.66	1440 (240)
$3d^3 4s$	$^3G_3$	15108	17901	2793	0.75	0.74	1350 (220)
$3d^3 4s$	$^3D_1$	17370	20683	3314	0.55	0.49	1180 (250)
$3d^3 4s$	$^3D_3$	17540	20925	3385	1.33	1.34	1430 (240)
$3d^3 4s$	$^3P_0$	17995	21261	3265			1220 (250)
$3d^3 4s$	$^3P_1$	18061	21391	3330	1.46		1350 (250)
$3d^3 4s$	$^3P_0$	18818	21982	3164			1550 (290)
$3d^3 4s$	$^3P_1$	18826	21968	3142	1.49		1510 (280)
$3d^4$	$^5D_0$	28773	32215	3442			580 (1420)
$3d^4$	$^3P_0$	34219	32300	−1919			1430 (1390)
$3d^2 4s4d$	$^5D_0$	41871	38130	−3742			1760 (310)
Odd Levels							
$3d^2 4s4p$	$^5G^o_2$	15877	15552	−325	0.33	0.34	200 (30)
$3d^2 4s4p$	$^5G^o_3$	15976	15681	−294	0.92	0.92	310 (40)
$3d^2 4s4p$	$^5F^o_1$	16817	16462	−355	0.00	0.00	390 (30)
$3d^2 4s4p$	$^5F^o_2$	16875	16538	−338	1.00	1.00	460 (40)
$3d^2 4s4p$	$^5F^o_3$	16961	16654	−307	1.25	1.25	560 (50)
$3d^2 4s4p$	$^5D^o_0$	18463	18180	282			00 (40)
$3d^2 4s4p$	$^5D^o_1$	**18483**	**18210**	**−273**	**1.50**	**1.50**	**520 (40)**
$3d^2 4s4p$	$^5D^o_2$	**18525**	**18275**	**−250**	**1.50**	**1.50**	**570 (40)**
$3d^2 4s4p$	$^5D^o_3$	**18594**	**18388**	**−206**	**1.50**	**1.50**	**660 (60)**
$3d^2 4s4p$	$^3F^o_2$	19323	19471	149	0.67	0.67	430 (40)
$3d^2 4s4p$	$^3F^o_3$	19422	19614	193	1.09	1.09	540 (50)
$3d^2 4s4p$	$^3D^o_1$	19938	20020	82	0.50	0.50	440 (60)
$3d^2 4s4p$	$^3D^o_2$	20006	20125	119	1.16	1.17	530 (30)
$3d^2 4s4p$	$^3D^o_3$	20126	20315	189	1.33	1.33	710 (60)
$3d^2 4s4p$	$^3G^o_3$	21469	22077	607	0.75	0.76	580 (50)
$3d^2 4s4p$	$^1D^o_2$	22081	22752	671	1.00	1.00	640 (100)
$3d^2 4s4p$	$^3S^o_1$	24921	25747	826	1.98	1.98	580 (460)
$3d^3 4p$	$^3D^o_1$	25318	26167	849	0.52	0.54	1000 (270)
$3d^2 4s4p$	$^3P^o_1$	25537	26337	800	1.50	1.48	490 (220)
$3d^2 4s4p$	$^3P^o_0$	25575	25649	74			640 (40)
$3d^2 4s4p$	$^5D^o_0$	25612	26303	690			450 (200)
$3d^3 4p$	$^5D^o_0$	29829	26589	−3240			640 (190)
$3d^2 4s4p$	$^3P^o_0$	31686	30955	−731			1740 (160)
$3d^3 4p$	$^3P^o_0$	33085	32811	−274			320 (350)

TABLE VII. **Scandium ($Z = 21$).** Comparison of experimental and calculated excitation energies, with calculated Landé g-factors, and $\delta\alpha$ sensitivity q-factors.

Leading config.	Term	Energy (cm^{-1}) Exp.[46]	Energy (cm^{-1}) Calc.	ΔE	Landé g Exp.[46]	Landé g Calc.	q (cm^{-1})
Even Levels							
$3d^2 4s$	$^2D_{3/2}$	0	0		0.80	0.80	
$3d^2 4s$	$^2D_{5/2}$	168	215	46	1.20	1.20	200 (60)
$3d^2 4s$	$^4F_{3/2}$	**11520**	**10919**	**−601**	**0.40**	**0.40**	**1050** (70)
$3d^2 4s$	$^4F_{5/2}$	**11558**	**10967**	**−590**	**1.03**	**1.03**	**1100** (**70**)
$3d^2 4s$	$^4F_{7/2}$	11610	11036	−574	1.24	1.24	1160 (80)
$3d^2 4s$	$^4F_{9/2}$	**11677**	**11130**	**−547**	**1.33**	**1.33**	**1250** (**80**)
$3d^2 4s$	$^2F_{5/2}$	14926	14548	−379	0.86	0.86	1180 (60)
$3d^2 4s$	$^2F_{7/2}$	15042	14703	−339	1.13	1.14	1320 (70)
$3d^2 4s$	$^2D_{5/2}$	17013	17190	177	1.23	1.28	990 (80)
$3d^2 4s$	$^2D_{3/2}$	17025	17218	193	0.82	0.90	1030 (70)
$3d^2 4s$	$^4P_{1/2}$	17226	17308	82	2.66	2.67	950 (90)
$3d^2 4s$	$^4P_{3/2}$	17255	17346	91	1.72	1.63	1010 (100)
$3d^2 4s$	$^4P_{5/2}$	17307	17431	124	1.58	1.52	1100 (60)
$3d^2 4s$	$^2G_{9/2}$	20237	20540	303	1.10	1.11	1040 (50)
$3d^2 4s$	$^2G_{7/2}$	20240	20544	304	0.89	0.89	1040 (60)
$3d^2 4s$	$^2P_{1/2}$	20681	20891	209	0.67	0.67	1120 (50)
$3d^2 4s$	$^2P_{3/2}$	20720	20941	221	1.33	1.33	1170 (50)
$3d^2 4s$	$^2S_{1/2}$	26937	27719	782		2.00	670 (90)
$3d^3$	$^4F_{7/2}$	33847	33588	−258	1.23	1.24	1670 (140)
$3d^3$	$^4F_{9/2}$	33906	33672	−234	1.33	1.33	1740 (130)
$3d4s5s$	$^4D_{1/2}$	34390	34015	−375	0.00	0.00	220 (0)
$3d4s5s$	$^4D_{7/2}$	34567	34242	−326	1.43	1.43	430 (10)
$3d^3$	$^4P_{1/2}$	36493	36511	19	2.63	2.65	1370 (710)
$3d^3$	$^2G_{9/2}$	37054	37204	150	1.11	1.11	1560 (410)
$3d^3$	$^2H_{9/2}$	39164	39369	205		0.91	1660 (1210)
Odd Levels							
$3d4s4p$	$^4F^o_{3/2}$	15673	15334	−338	0.43	0.44	160 (10)
$3d4s4p$	$^4F^o_{5/2}$	15757	15433	−324	1.04	1.05	250 (10)
$3d4s4p$	$^4F^o_{7/2}$	15882	15585	−297	1.23	1.24	400 (20)
$3d4s4p$	$^4D^o_{1/2}$	16010	15587	−423	0.00	0.00	340 (20)
$3d4s4p$	$^4D^o_{3/2}$	16022	15617	−405	1.04	1.13	380 (40)
$3d4s4p$	$^2D^o_{5/2}$	16023	15658	−365	1.19	1.27	430 (10)
$3d4s4p$	$^4F^o_{9/2}$	16027	15744	−283	1.33	1.33	570 (20)
$3d4s4p$	$^2D^o_{3/2}$	**16097**	**15772**	**−325**	**0.96**	**0.83**	**530** (**40**)
$3d4s4p$	$^4D^o_{5/2}$	16141	15779	−362	1.34	1.28	530 (20)
$3d4s4p$	$^4D^o_{7/2}$	**16211**	**15828**	**−383**	**1.43**	**1.43**	**580** (**20**)
$3d4s4p$	$^4P^o_{1/2}$	18504	18206	−298	2.53	2.64	390 (40)
$3d4s4p$	$^4P^o_{3/2}$	18516	18232	−284	1.70	1.72	390 (140)
$3d4s4p$	$^4P^o_{5/2}$	18571	18303	−269	1.60	1.60	490 (10)
$4s^2 4p$	$^2P^o_{1/2}$	18711	18743	32	0.78	0.69	−390 (280)
$4s^2 4p$	$^2P^o_{3/2}$	18856	18889	34	1.36	1.34	−200 (230)
$3d4s4p$	$^2F^o_{5/2}$	21033	20946	−87	0.86	0.86	560 (10)
$3d4s4p$	$^2F^o_{7/2}$	21086	20995	−91	1.14	1.14	610 (10)
$3d4s4p$	$^2P^o_{1/2}$	24657	24618	−39		0.67	420 (90)
$3d4s4p$	$^2F^o_{7/2}$	25725	25291	−434	1.14	1.14	840 (90)
$3d^2 4p$	$^4G^o_{7/2}$	29096	28079	−1017	0.98	0.98	1440 (70)
$3d^2 4p$	$^4G^o_{9/2}$	29190	28190	−1000	1.16	1.17	1540 (70)
$3d4s4p$	$^2P^o_{1/2}$	30573	30601	28	0.68	0.67	−190 (180)
$3d^2 4p$	$^4F^o_{9/2}$	31351	30297	−1054	1.33	1.33	1680 (80)
$3d^2 4p$	$^2G^o_{9/2}$	33151	32290	−862	1.06	1.11	1680 (70)
$3d^2 4p$	$^2H^o_{9/2}$	39153	39092	−61		1.04	1450 (780)

TABLE VIII. **Calcium ($Z = 20$).** Comparison of experimental and calculated excitation energies, and calculated q-factors.

Leading		Energy (cm^{-1})			
config.	Term	Exp.[46]	Calc.	ΔE	q (cm^{-1})
Even Levels					
$4s^2$	$^1S_0$	0	0		0
$3d4s$	$^3D_1$	20335	20325	−10	740 (25)
$3d4s$	$^3D_2$	20349	20350	1	760 (26)
$3d4s$	$^1D_2$	21850	22044	195	780 (32)
$4s5s$	$^3S_1$	31539	31704	164	130 (2)
$4s5s$	$^1S_0$	33317	33524	207	141 (2)
$4s4d$	$^1D_2$	37298	37506	208	370 (22)
$4s4d$	$^3D_1$	**37748**	**37932**	**184**	**243 (1)**
$4s4d$	$^3D_2$	37752	37937	185	247 (2)
$4p^2$	$^3P_0$	38418	38744	327	580 (40)
$4p^2$	$^3P_1$	38465	38795	330	640 (39)
$4p^2$	$^3P_2$	38552	38887	336	730 (36)
$4s6s$	$^3S_1$	40474	40604	129	150 (2)
$4s6s$	$^1S_0$	40690	40844	153	330 (140)
$4p^2$	$^1D_2$	40720	40919	199	690 (56)
$4p^2$	$^1S_0$	41786	42019	233	620 (100)
$4s5d$	$^3D_1$	42743	42919	176	204 (7)
$4s5d$	$^3D_2$	42745	42921	177	210 (500)
$4s7s$	$^3S_1$	43981	44235	255	156 (3)
$4s7s$	$^1S_0$	44277	44610	333	177 (7)
$4s8s$	$^1S_0$	45887	47669	1782	170 (500)
Odd Levels					
$4s4p$	$^3P^o_0$	15158	15398	240	132 (3)
$4s4p$	$^3P^o_1$	15210	15453	243	187 (3)
$4s4p$	$^3P^o_2$	15316	15565	249	298 (5)
$4s4p$	$^1P^o_1$	23652	23758	106	290 (9)
$3d4p$	$^3F^o_2$	35730	35891	161	1060 (170)
$3d4p$	$^1D^o_2$	35835	35780	−56	980 (330)
$4s5p$	$^3P^o_0$	36548	36682	134	250 (56)
$4s5p$	$^3P^o_1$	36555	36690	136	260 (55)
$4s5p$	$^3P^o_2$	36575	36714	139	280 (360)
$4s5p$	$^1P^o_1$	36732	36911	180	320 (29)
$3d4p$	$^3D^o_1$	38192	38173	−19	1100 (19)
$3d4p$	$^3D^o_2$	38219	38212	−7	1130 (20)
$3d4p$	$^3P^o_0$	39333	39412	79	970 (27)
$3d4p$	$^3P^o_1$	39335	39422	87	980 (27)
$3d4p$	$^3P^o_2$	39340	39444	104	990 (29)
$4s6p$	$^1P^o_1$	41679	41847	168	410 (94)
$4s4f$	$^3F^o_2$	**42170**	**42430**	**260**	**170 (19)**
$4s6p$	$^3P^o_0$	42515	42670	155	180 (14)
$4s7p$	$^3P^o_0$	44956	45530	575	163 (3)
$4s8p$	$^3P^o_0$	46284	48852	2568	160 (500)

TABLE IX. **Silicon ($Z = 14$).** Comparison of experimental and calculated excitation energies, and calculated q-factors.

Leading config.	Term	Energy (cm^{-1}) Exp.[46]	Calc.	ΔE	q (cm^{-1})
Even Levels					
$3s^2 3p^2$	$^3P_0$	0	0		
$3s^2 3p^2$	$^3P_1$	77	18	−59	85 (4)
$3s^2 3p^2$	$^3P_2$	223	186	−37	240 (9)
$3s^2 3p^2$	$^1D_2$	6299	6456	157	160 (10)
$3s^2 3p^2$	$^1S_0$	15394	15640	245	170 (10)
$3s^2 3p4p$	$^1P_1$	47284	47024	−260	39 (5)
$3s^2 3p4p$	$^3D_1$	48020	47738	−282	−62 (6)
$3s^2 3p4p$	$^3D_2$	48102	47827	−275	2 (4)
$3s^2 3p4p$	$^3P_0$	49028	48784	−245	−42 (3)
$3s^2 3p4p$	$^3P_1$	49061	48803	−257	−21 (13)
$3s^2 3p4p$	$^3P_2$	49189	48946	−243	140 (9)
$3s^2 3p4p$	$^3S_1$	49400	49112	−288	146 (5)
$3s^2 3p4p$	$^1D_2$	**50189**	**49997**	**−192**	**100 (11)**
$3s^2 3p4p$	$^1S_0$	51612	51548	−64	95 (10)
$3s^2 3p5p$	$^1P_1$	56780	58674	1894	−33 (18)
$3s^2 3p5p$	$^3D_2$	57017	58929	1912	−31 (12)
$3s^2 3p5p$	$^3P_0$	57296	59225	1930	−53 (10)
$3s^2 3p5p$	$^1S_0$	58312	60212	1901	120 (20)
Odd Levels					
$3s^3 p3$	$^5S^o_2$	33326	33348	22	580 (20)
$3s^2 3p4s$	$^3P^o_0$	39683	39418	−265	−157 (3)
$3s^2 3p4s$	$^3P^o_1$	39760	39504	−257	−90 (3)
$3s^2 3p4s$	$^3P^o_2$	39955	39707	−248	130 (10)
$3s^2 3p4s$	$^1P^o_1$	40992	40764	−227	69 (13)
$3s^3 p3$	$^3D^o_1$	45276	45715	438	330 (20)
$3s^3 p3$	$^3D^o_2$	45294	45687	393	350 (20)
$3s^2 3p3d$	$^1D^o_2$	47352	47552	201	140 (10)
$3s^2 3p3d$	$^3F^o_2$	49851	49930	79	−24 (9)
$3s^2 3p3d$	$^3P^o_2$	50500	50558	58	150 (15)
$3s^2 3p3d$	$^3P^o_1$	50566	50673	107	220 (15)
$3s^2 3p3d$	$^3P^o_0$	50602	50679	77	260 (20)
$3s^2 3p3d$	$^1P^o_1$	53387	53213	−174	56 (12)
$3s^2 3p3d$	$^3D^o_1$	54185	54056	−130	−86 (5)
$3s^2 3p5s$	$^3P^o_0$	54245	53982	−263	−139 (3)
$3s^2 3p5s$	$^3P^o_1$	54314	54344	30	150 (20)
$3s^2 3p5s$	$^1P^o_1$	**54871**	**54665**	**−206**	**130 (20)**
$3s^2 3p4d$	$^3P^o_0$	56733	57702	969	310 (60)
$3s^2 3p6s$	$^3P^o_0$	59221	61135	1914	−120 (10)
$3s^2 3p4d$	$^3P^o_0$	60043	61752	1709	230 (10)

TABLE X. **Sodium ($Z = 11$).** Comparison of experimental and calculated excitation energies, and calculated q-factors.

State		Energy (cm^{-1}) Exp. [46]	Calc.	ΔE	q (cm^{-1})
Even Levels					
$3s$	$^2S_{1/2}$	0	0		0
$\boldsymbol{4s}$	$\boldsymbol{^2S_{1/2}}$	**25740**	**25661**	**−79**	**45 (3)**
Odd Levels					
$3p$	$^2P^o_{1/2}$	16956	16860	−96	45 (3)
$3p$	$^2P^o_{3/2}$	16973	16878	−95	64 (4)
$\boldsymbol{4p}$	$\boldsymbol{^2P^o_{1/2}}$	**30267**	**30161**	**−106**	**54 (3)**
$\boldsymbol{4p}$	$\boldsymbol{^2P^o_{3/2}}$	**30273**	**30167**	**−106**	**60 (4)**

TABLE XI. Transition frequencies, and calculated q and k sensitivity coefficients.

Lower		Upper		(cm^{-1}) ω [46]	q	(Å) λ	k_α
Y ($Z=39$)							
$4d^2 5s$	$^4F_{7/2}$	$4d5s5p$	$^4F^o_{7/2}$	4434.6	−1950(130)	22549.938	−0.88(6)
Fe ($Z=26$)							
$3d^6 4s^2$	$^3D_3$	$3d^6 4s4p$	$^3P^o_2$	4575.1	1284(650)	21857.345	0.56(28)
Ti ($Z=22$)							
$3d^3 4s$	$^5P_1$	$3d^2 4s4p$	$^5D^o_2$	4543.3	−720(210)	22010.501	−0.31(9)
$3d^3 4s$	$^5P_2$	$3d^2 4s4p$	$^5D^o_1$	4454.3	−820(220)	22450.025	−0.37(10)
		$3d^2 4s4p$	$^5D^o_2$	4496.6	−770(220)	22238.911	−0.34(10)
		$3d^2 4s4p$	$^5D^o_3$	4565.5	−680(230)	21903.353	−0.30(10)
Sc ($Z=21$)							
$3d^2 4s$	$^4F_{3/2}$	$3d4s4p$	$^2D^o_{3/2}$	4576.9	−520(80)	21848.743	−0.23(3)
$3d^2 4s$	$^4F_{5/2}$	$3d4s4p$	$^2D^o_{3/2}$	4539.2	−570(80)	22030.179	−0.25(4)
$3d^2 4s$	$^4F_{9/2}$	$3d4s4p$	$^4D^o_{7/2}$	4533.5	−670(80)	22058.003	−0.29(4)
Ca ($Z=20$)							
$4s4d$	$^3D_1$	$4s4f$	$^3F^o_2$	4422.0	−73(19)	22614.115	−0.03(1)
Si ($Z=14$)							
$3s^2 3p4p$	$^1D_2$	$3s^2 3p5s$	$^1P^o_1$	4681.6	30(21)	21360.027	0.013(9)
Na ($Z=11$)							
$4s$	$^2S_{1/2}$	$4p$	$^2P^o_{1/2}$	4527.0	9(5)	22089.728	0.004(2)
		$4p$	$^2P^o_{3/2}$	4532.6	15(5)	22062.485	0.007(2)